

Increased H3K9me3 drives dedifferentiated phenotype via KLF6 repression in liposarcoma

Emily Z. Keung,^{1,2,3} Kadir C. Akdemir,¹ Ghadah A. Al Sannaa,⁴ Jeannine Garnett,² Dina Lev,⁵ Keila E. Torres,² Alexander J. Lazar,⁴ Kunal Rai,¹ and Lynda Chin¹

¹Department of Genomic Medicine and ²Department of Surgical Oncology, The University of Texas MD Anderson Cancer Center, Houston, Texas, USA. ³Department of Surgery, Brigham and Women's Hospital, Harvard Medical School, Boston, Massachusetts, USA. ⁴Department of Pathology, The University of Texas MD Anderson Cancer Center, Houston, Texas, USA. ⁵Department of Surgery, Sheba Medical Center, Tel Aviv, Israel.

Liposarcoma (LPS) can be divided into 4 different subtypes, of which well-differentiated LPS (WDLPS) and dedifferentiated LPS (DDLPS) are the most common. WDLPS is typically low grade, whereas DDLPS is high grade, aggressive, and carries a worse prognosis. WDLPS and DDLPS frequently co-occur in patients. However, it is not clear whether DDLPS arises independently from WDLPS, or whether epigenomic alterations underly the histopathological differences of these subtypes. Here, we profiled 9 epigenetic marks in tumor samples from 151 patients with LPS and showed elevated trimethylation of histone H3 at Lys9 (H3K9me3) levels in DDLPS tumors. Integrated CHIP-seq and gene expression analyses of patient-derived cell lines revealed that H3K9me3 mediates differential regulation of genes involved in cellular differentiation and migration. Among these, Kruppel-like factor 6 (*KLF6*) was reduced in DDLPS, with increased H3K9me3 at associated regulatory regions. Pharmacologic inhibition of H3K9me3 with chaetocin decreased DDLPS proliferation and increased expression of the adipogenesis-associated factors *PPAR γ* , *CEBP α* , and *CEBP β* , suggesting that increased H3K9me3 may mediate DDLPS-associated aggressiveness and dedifferentiation properties. *KLF6* overexpression partially phenocopied chaetocin treatment in DDLPS cells and induced phenotypic changes that were consistent with adipocytic differentiation, suggesting that the effects of increased H3K9me3 may be mediated through *KLF6*. In conclusion, we provide evidence of an epigenetic basis for the transition between WDLPS and DDLPS.

Introduction

Liposarcoma (LPS) is one of the most common subtypes of soft tissue sarcoma, accounting for 24% of extremity and 45% of retroperitoneal soft tissue sarcomas (1). There are 4 recognized LPS subtypes, with well differentiated (WD) and dedifferentiated (DD) histologies being the most common. Whereas WDLPS are low-grade tumors that typically have a more indolent course, DDLPS are high-grade, aggressive tumors with a systemic metastatic rate of 5% to 20% (1) and a considerably worse patient prognosis (2). Surgical excision remains the standard of care for localized disease, as these tumors are largely resistant to conventional cytotoxic therapies. Nevertheless, 58% to 80% of patients with DDLPS of the retroperitoneum will succumb to locally recurrent or metastatic disease within 5 years (3). Thus, gaining a better understanding of the pathogenesis of WDLPS and DDLPS is a critical first step toward the development of effective targeted therapies to improve outcomes in patients with this disease.

Currently, the pathogenesis of WDLPS and DDLPS is poorly understood. Whether DDLPS arises from WDLPS or independently is unknown. WDLPS and DDLPS often occur synchronously or metachronously in patients and show similar cytogenetic features (4). Both are characterized by amplification of chromosome

12q14-15, the best-studied molecular aberration in LPS (2, 5-7), which results in amplification of the *MDM2* gene (located at 12q15) in 100% of cases and *CDK4* in 90% of cases (5). Amplification of 12q14-15 is associated with decreased apoptosis and increased cell proliferation, which is thought to be mediated by dysregulation of the p53 pathway and the Rb-E2F cell cycle checkpoint. Currently, *MDM2* and *CDK4* are being targeted by small-molecule inhibitors (RG 7112, flavoperidol, PD0332991) which have shown promising activity in a small number of preclinical and phase I and II clinical studies (7-11). In the past decade, several groups have also undertaken gene expression profiling, DNA copy number profiling, whole-exome sequencing, miR profiling, and RNA sequencing approaches toward expanding our understanding of LPS pathogenesis (3, 12-15). These efforts have implicated a number of miRs (miRs 143, 155, and 193b), which constitute a mechanism of epigenetic gene regulation, and potential downstream pathways as being involved in liposarcomagenesis (3, 13, 15).

In recent years, it has become increasingly evident that epigenetic deregulation plays critical roles in human disease, including cancers (16, 17). Epigenetic processes may play important roles in liposarcomagenesis, as suggested by 2 recent studies focused on DNA methylation profiling of LPS (3, 18). Whereas Renner et al. (18) suggested *NNAT* (neuronatin) as a potential tumor suppressor in myxoid LPS using DNA methylation and gene expression profiling of 80 sarcomas of mixed histologies (of which 12 were DDLPS), Taylor et al. (3) reported epigenetic aber-

Conflict of interest: The authors have declared that no conflict of interest exists.

Submitted: July 15, 2014; **Accepted:** June 4, 2015.

Reference information: *J Clin Invest.* 2015;125(8):2965-2978. doi:10.1172/JCI177976.

Table 1. H3K9me3 is differentially expressed in WDLPS and DDLPS tumors

Epigenetic mark	Score	WD (n = 415)	DD (n = 157)	P value
		mean (median, range)	mean (median, range)	
H3K9me3	Intensity	<u>0.63 (1, 0–2)</u>	<u>0.78 (1, 0–2)</u>	0.029
	Percent	<u>17.34 (5, 0–80)</u>	<u>24.17 (10, 0–80)</u>	0.006
	Mult	<u>22.94 (5, 0–140)</u>	<u>32.99 (10, 0–140)</u>	0.009
5mC	Intensity	1.88 (2, 0–3)	1.74 (2, 0–3)	0.005
	Percent	59.48 (60, 0–90)	63.22 (60, 0–100)	<0.001
	Mult	114.02 (120, 0–270)	115.07 (120, 0–270)	0.244
5hmC	Intensity	1.57 (2, 0–2)	1.31 (1, 1–2)	<0.001
	Percent	72.48 (70, 0–100)	72.34 (80, 5–100)	0.403
	Mult	115.46 (120, 0–200)	96.61 (80, 5–200)	<0.001
H3K27Ac	Intensity	1.63 (2, 0–3)	1.79 (2, 0–3)	0.074
	Percent	50.48 (60, 0–100)	61.63 (60, 0–90)	<0.001
	Mult	96.45 (120, 0–240)	115.66 (120, 0–210)	<0.001
H3K27me3	Intensity	1.07 (1, 0–2)	0.99 (1, 0–2)	0.168
	Percent	37.64 (40, 0–90)	35.49 (40, 0–90)	0.618
	Mult	55.54 (50, 0–180)	45.49 (40, 0–180)	0.133
H3K4me3	Intensity	1.41 (2, 0–3)	1.47 (2, 0–2)	0.894
	Percent	51.31 (60, 0–90)	61.6 (80, 0–90)	<0.001
	Mult	89.93 (100, 0–240)	98.47 (100, 0–180)	0.201
H3K20me3	Intensity	1.45 (2, 0–2)	1.39 (1, 0–3)	0.173
	Percent	56.74 (60, 0–90)	57.73 (60, 0–90)	0.641
	Mult	94.31 (100, 0–180)	57.73 (60, 0–90)	0.330
H3K36me2	Intensity	1.14 (1, 0–2)	1.06 (1, 0–2)	0.086
	Percent	46 (50, 0–90)	60.25 (55, 0–180)	0.006
	Mult	60.25 (55, 0–180)	62.31 (60, 0–180)	0.321
H3K79me3	Intensity	1.63 (2, 0–2)	1.35 (1, 0–2)	<0.001
	Percent	66.89 (70, 0–90)	64.14 (70, 0–90)	0.409
	Mult	111.78 (120, 0–180)	91.04 (80, 0–180)	<0.001

Global expression of 9 epigenetic marks in human WDLPS and DDLPS tumors by immunohistochemical analysis of a TMA of WDLPS and DDLPS tumors from 151 unique patients. Cores were assigned a score for intensity of tumor nuclei staining (Intensity), percentage of tumor nuclei stained (Percent), and a third score derived by multiplying the intensity and percentage scores (Mult). Data were analyzed by Student's *t* test. Bold text indicates statistical significance ($P < 0.05$); underlined text highlights H3K9me3 data.

rations associated with the promoters of *CEBPA* and miR-193b in a subset of DDLPS tumors profiled. However, a comprehensive understanding of the different epigenetic modifications that occur has been lacking. An unbiased and systematic approach is needed to examine epigenetic modifications and their contribution to liposarcomagenesis, specifically DDLPS.

In this study, we explored the epigenomic differences between WDLPS and DDLPS in cell-based systems and human tumor samples using unbiased approaches. We identified and validated Kruppel-like factor 6 (KLF6) as an H3K9me3-controlled and differentially expressed transcription factor serving a previously unappreciated tumor-suppressor role in LPS. Mechanistically, KLF6 may drive adipocytic differentiation through increased expression of known regulators of adipogenesis including PPAR γ , thereby leading to the observed phenotypic changes associated with cellular differentiation and senescence.

Results

H3K9me3 is differentially marked in WDLPS and DDLPS tumors. To gain insight into the role of epigenetic regulation during liposarcomagenesis, we examined the global levels of 7 his-

tone marks (H3K4me3, H3K27Ac, H3K36me2, H3K79me3, H3K9me3, H3K20me3, and H3K27me3) and 2 DNA methylation marks (5-methylcytosine, 5mC and 5-hydroxymethylcytosine, 5hmC) known to be important in the regulation of gene expression (16, 17, 19, 20). Of these, H3K9me3, H3K20me3, H3K27me3, and 5mC are associated with gene repression, whereas H3K4me3, H3K27Ac, H3K36me2, and H3K79me3 are associated with gene activation. In particular, H3K4me3 marks active promoters, H3K27Ac marks active enhancers, and H3K36me2 and H3K79me3 mark transcribed genes (16, 17, 19, 20). Optimal dilutions for immunohistochemical studies using Encyclopedia of DNA Elements–validated (ENCODE-validated) antibodies against these marks were first determined (data not shown). For each of these 9 antibodies, we performed immunohistochemical analysis of a tissue microarray (TMA) containing WDLPS and DDLPS tumors surgically resected from 151 unique patients (Supplemental Figure 1; supplemental material available online with this article; doi:10.1172/JCI77976DS1). TMA cores were scored by assigning a mean stain intensity score (0 = negative, 1 = low, 2 = intermediate, 3 = high) (Supplemental Figure 2) as well as a percentage of tumor cells stained (0%–100%).

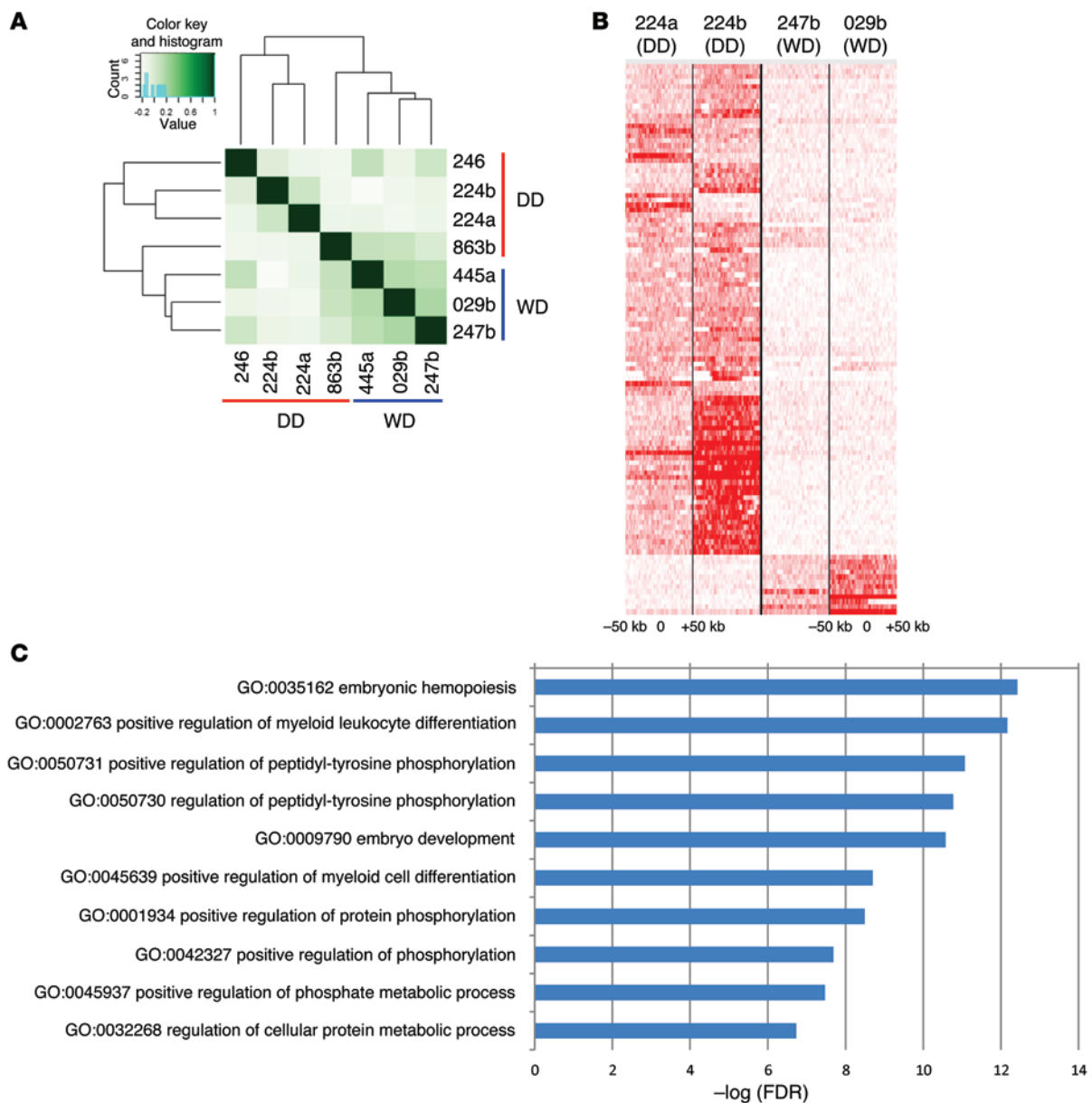


Figure 1. Results of H3K9me3 ChIP-seq in WDLPS and DDLPS cell lines. (A) Unsupervised clustering of WDLPS and DDLPS cell lines by regions of H3K9me3 enrichment. (B) Heatmap of H3K9me3-binding signals approximately 50 kb upstream and downstream of regions that were differentially enriched between DDLPS and WDLPS cell lines. (C) Top 10 GO terms identified for genes associated with differential H3K9me3 enrichment between DDLPS and WDLPS cell lines. Level of significance ($-\log$ of the FDR value) is plotted for each GO term. Hypergeometric tests were used.

Each core was additionally assigned a multiplier score derived by multiplying its mean stain intensity score and the percentage of tumor cells stained.

We found statistically significant associations between LPS histology and some of the chromatin marks investigated. DDLPS were associated with higher levels of the established repressive mark H3K9me3, higher levels of the active enhancer mark H3K27Ac, and lower levels of H3K79me3 and 5hmC, an intermediate associated with DNA demethylation (Table 1). That H3K9me3 and DNA methylation marks appeared to be coordinately differentially expressed among WDLPS and DDLPS tumors is consistent with the known crosstalk between DNA methylation and H3K9me3 histone modification pathways. Although DNA

methylation and histone modifications are carried out by different sets of enzymes, these modifications have been shown to influence each other in a bidirectional manner, and this crosstalk may be mediated, at least in part, through direct interactions between histone and DNA methyltransferases (19–21). As no prior knowledge is available on the role of histone modifications in LPS, we elected to focus our investigations on the role of H3K9me3 modification in this disease.

Identifying regions of differential H3K9me3 expression in WDLPS and DDLPS cell lines. We hypothesized that differential H3K9me3 enrichment at specific loci in the genomes of WDLPS and DDLPS might result in dysregulation of gene expression and contribute to the transition from WDLPS to DDLPS. Using 7 cell lines derived from

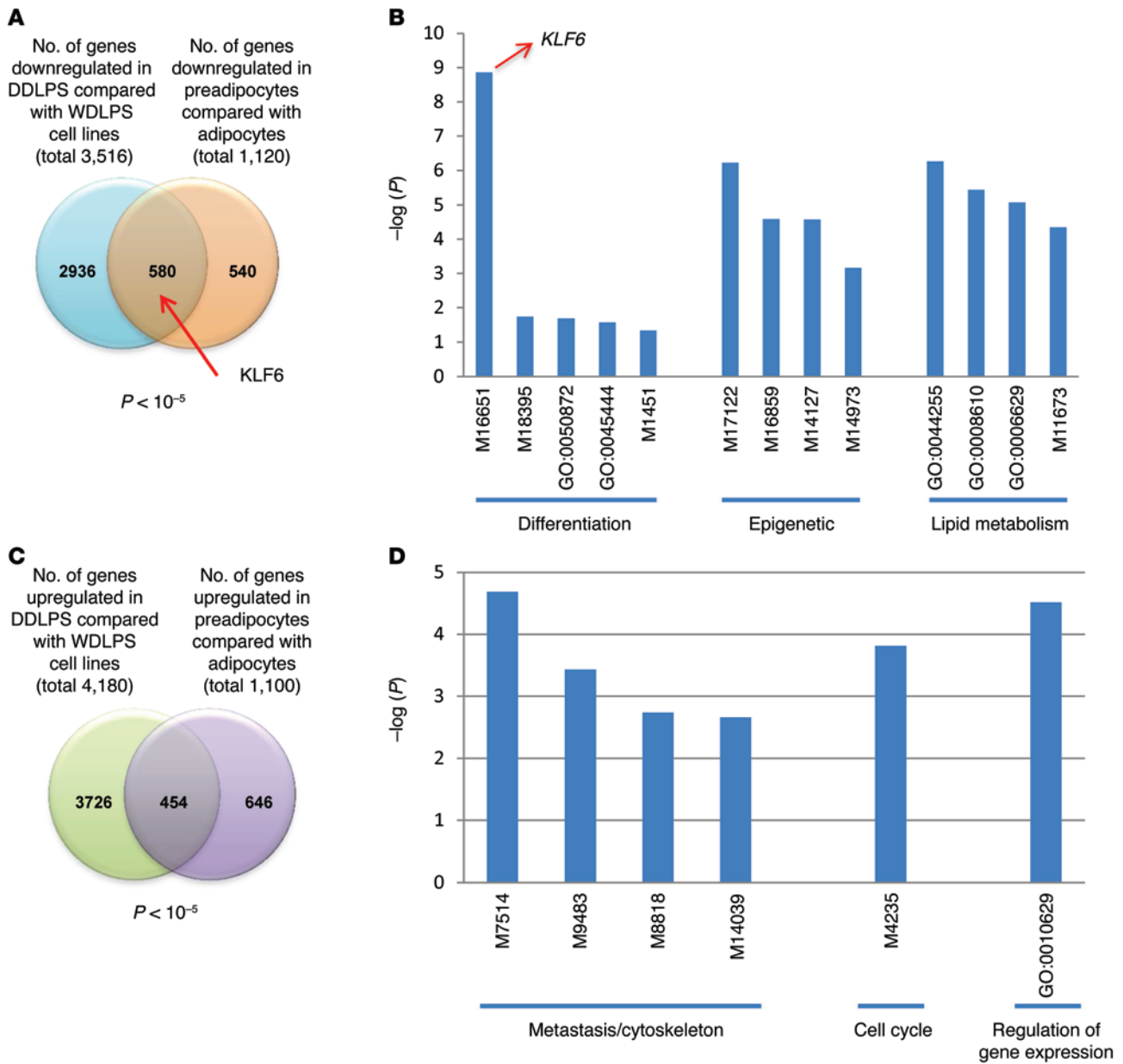


Figure 2. Gene expression profiling of WDLPS and DDLPS cell lines. (A) Number of distinct and overlapping differentially downregulated genes in DDLPS cell lines (versus WDLPS cell lines) and preadipocytes (versus adipocytes). (B) Functional annotation of common differentially downregulated genes in DDLPS cell lines (versus WDLPS cell lines) and preadipocytes (versus adipocytes). (C) Number of distinct and overlapping differentially upregulated genes in DDLPS cell lines (versus WDLPS cell lines) and preadipocytes (versus adipocytes). (D) Functional annotation of common differentially upregulated genes in DDLPS cell lines (versus WDLPS cell lines) and preadipocytes (versus adipocytes). The level of significance ($-\log$ of the P value) is plotted for each MSigDB or GO term. *KLF6* is among the target genes in the listed terms. Hypergeometric tests were used.

human WDLPS and DDLPS tumors (Supplemental Materials and Methods), independent of those represented on the TMA (Supplemental Figure 3), we performed ChIP, followed by deep sequencing (ChIP-seq), using the ENCODE-validated H3K9me3 antibody to define genomic loci with enrichment of H3K9me3 in each cell line. The total number of reads per cell line sequenced ranged between 18 and 22 million (Supplemental Figure 4A). Enrichment analysis showed that cell lines contained between 434 and 2,075 sites that are significantly enriched in the 7 cell line-derived samples compared with the corresponding whole-cell extract DNA (input). Using these identified regions, we performed unsupervised hierarchical

clustering of the 7 cell lines (Figure 1A). Despite the expected heterogeneity observed among the 7 cell lines, cell lines derived from DDLPS tumors and those derived from WDLPS tumors clustered together, reinforcing the notion that global patterns of epigenomic marks are different between WDLPS and DDLPS.

To identify regions of differential H3K9 methylation, we focused on WDLPS cell lines 247b and 029b and DDLPS cell lines 224a and 224b, as these cell lines showed the strongest intra-subtype correlation (Figure 1A). We identified 243 regions enriched for H3K9me3 in DDLPS samples compared with WDLPS samples (Supplemental Figure 4B) and 17 regions enriched in

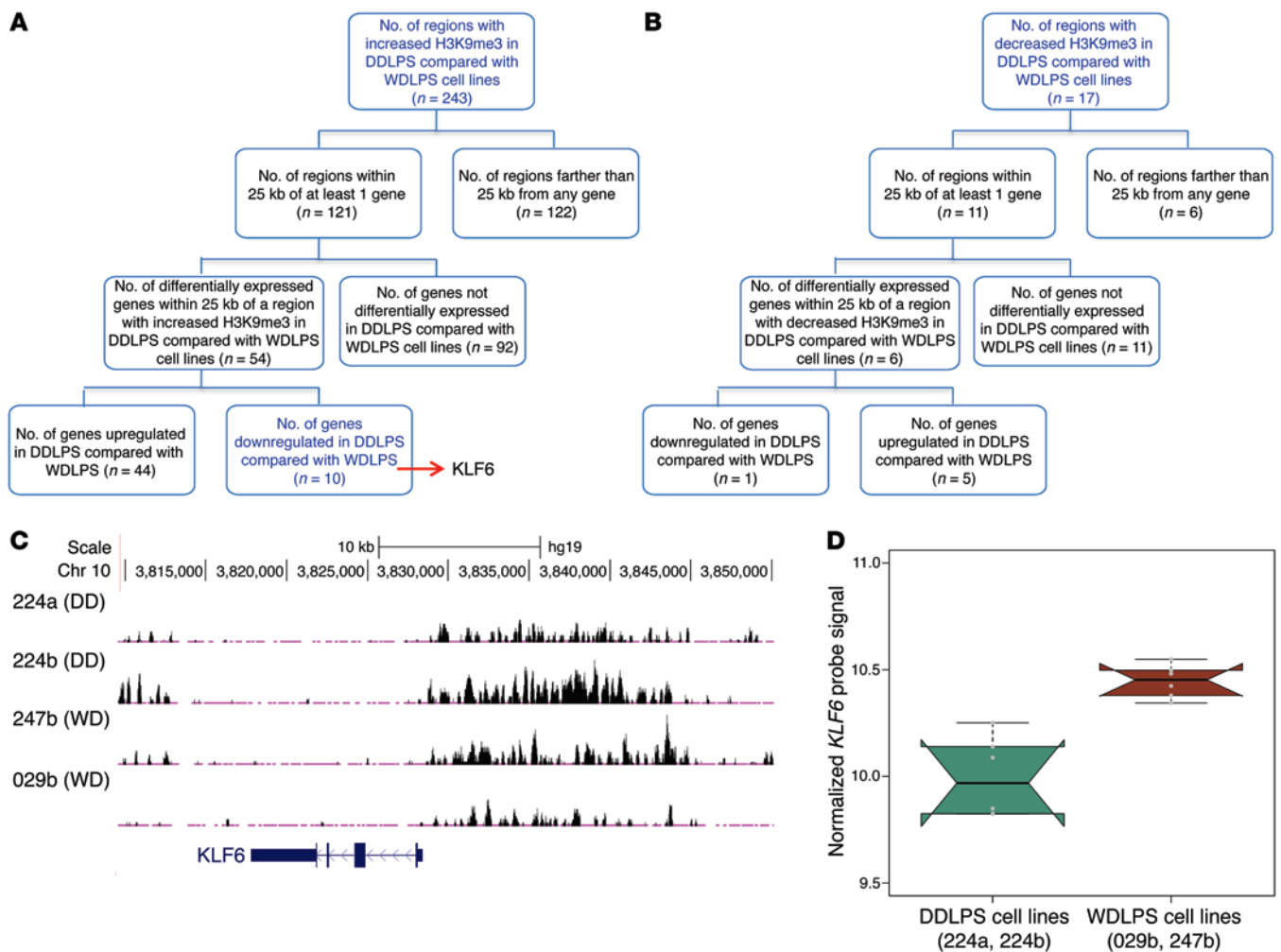


Figure 3. *KLF6* is epigenetically silenced in DDLPS. (A) Number of distinct and overlapping genes associated with increased H3K9me3 enrichment and decreased expression in DDLPS cell lines compared with WDLPS cell lines. (B) Number of distinct and overlapping genes associated with decreased H3K9me3 enrichment and increased expression in DDLPS cell lines compared with WDLPS cell lines. (C) Histograms of ChIP fragments across the *KLF6* locus for each LPS cell line. Each track is normalized to 10 million reads with the same track height and vertical viewing range. Chr, chromosome. (D) Box plot showing *KLF6* expression in DDLPS cell lines (224a, 224b) compared with WDLPS cell lines (029b, 247b) by microarray analysis ($n = 3$).

WDLPS samples compared with DDLPS samples (Supplemental Figure 4C). Accordingly, a heatmap plot showed signal differences in H3K9me3 at the identified genomic regions (Figure 1B). Similarly, we generated aggregate plots to visualize cell line-specific H3K9me3 enrichment across the aforementioned genomic loci in Figure 1B (Supplemental Figure 4, D and E).

In order to understand the functional relevance of differential H3K9me3 enrichment at specific observed regions between DDLPS and WDLPS cell lines, we performed gene set enrichment analysis (GSEA) using the Genomic Regions Enrichment of Annotations Tool (GREAT) (22). The top gene ontology (GO) terms thus identified revealed pathways involved in cellular differentiation and migration (Figure 1C and Supplemental Table 1). We also integrated our H3K9me3 ChIP-seq data set with locations of adipocyte super-enhancer domains (H3K27Ac ChIP-seq data from Young et al., ref. 23) and found notable overlap between regions of increased H3K9me3 enrichment in DDLPS cell lines relative to WDLPS cell lines ($n = 243$) and adipocyte-associated enhancers and super-enhancer regions ($n = 52$). Of these 52 regions, 13

were super-enhancer regions. Together, these data suggest that H3K9me3 may regulate aggressiveness in LPS and block the maintenance of normal adipocytic differentiation through its effect on key genes that control cell state and identity as well as associated regulatory elements such as super-enhancers.

Next, to gain insight into the differentiation pathways that differ between WDLPS and DDLPS, we performed transcriptome profiling of WDLPS and DDLPS cell lines using the Affymetrix U133A GeneChip array and identified 7,694 differentially expressed genes (FDR < 0.05) (Supplemental Figure 5 and Supplemental Table 2). Of these, 3516 genes were downregulated in DDLPS cell lines compared with WDLPS cell lines, while 4,180 genes were upregulated in DDLPS cell lines compared with WDLPS cell lines. We next performed GSEA of differentially expressed genes in DDLPS cell lines compared with WDLPS cell lines using HOMER (24). Of interest, genes related to a number of gene sets pertaining to cellular differentiation, lipid metabolism, epigenetic enzyme targets, metastasis, cell cycle, and miRs were differentially expressed between DDLPS and WDLPS cell lines (Supplemental Tables 3 and 4).

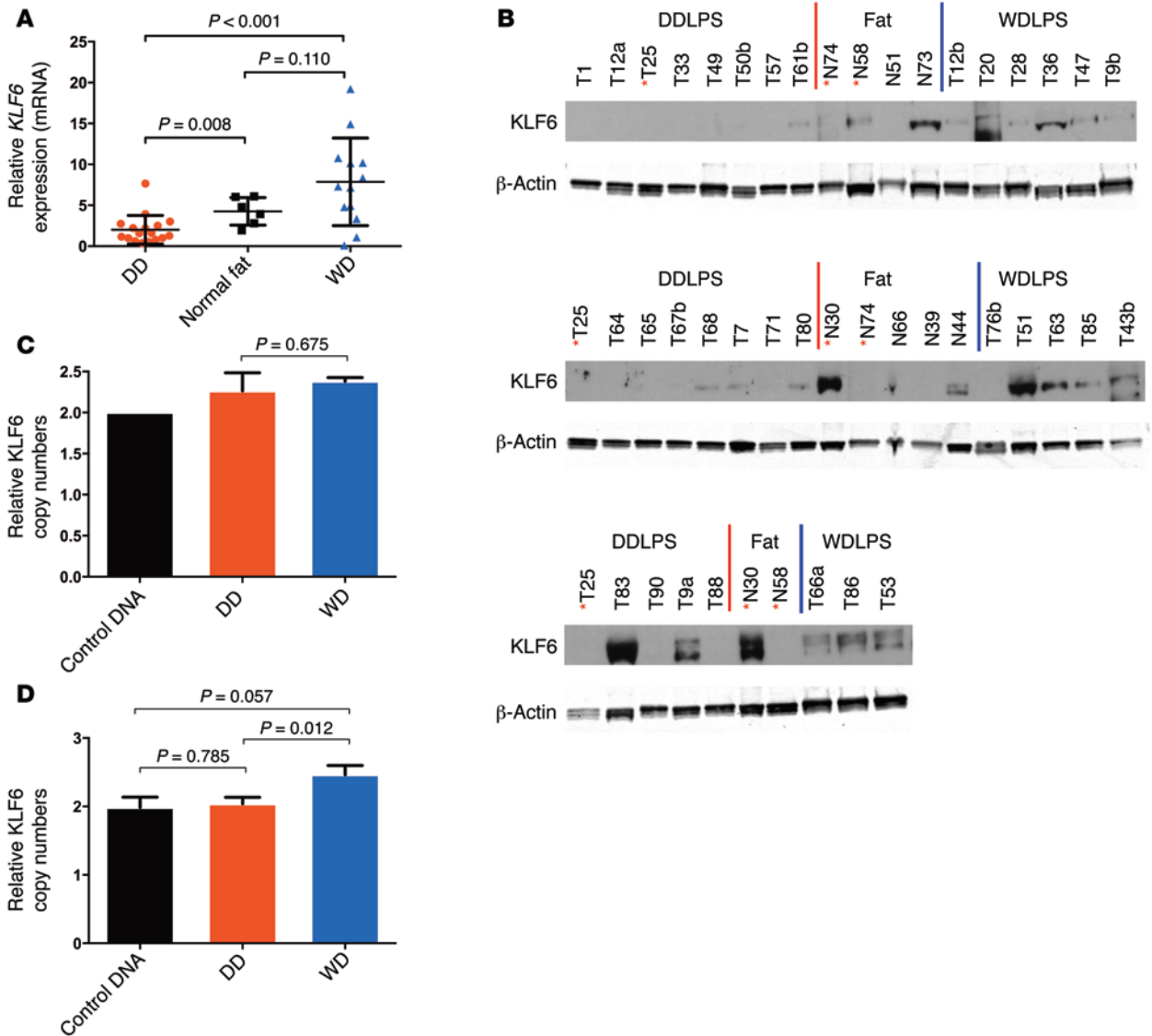


Figure 4. KLF6 is underexpressed in human DDLPS tumors compared with WDLPS tumors. (A) *KLF6* expression levels in human DDLPS tumors ($n = 17$) compared with those detected in WDLPS tumors ($n = 13$) and normal fat ($n = 6$), as assessed by qRT-PCR normalized to *GAPDH* (mean \pm SD; $n = 3$). Data were analyzed by Mann-Whitney *U* and Kruskal-Wallis tests. (B) *KLF6* protein expression in human DDLPS tumors ($n = 19$) compared with levels detected in normal fat ($n = 8$) and WDLPS tumors ($n = 14$), as assessed by Western blot analysis. (C) Relative *KLF6* copy numbers of WDLPS ($n = 3$) and DDLPS ($n = 4$) cell lines, as assessed by TaqMan CNV assay (RNaseP reference) (mean \pm SD; $n = 3$). Data were analyzed by the Mann-Whitney *U* test. (D) Relative *KLF6* copy numbers of WDLPS ($n = 15$) and DDLPS ($n = 19$) tumors, as assessed by TaqMan CNV assay (RNaseP reference) (mean \pm SD; $n = 3$). Data were analyzed by Mann-Whitney *U* and Kruskal-Wallis tests. Mean *KLF6* copy number: normal fat specimens, 1.99 (95% CI 1.60–2.37), DDLPS tumors, 2.04 (95% CI 1.84–2.24), and WDLPS tumors, 2.46 (95% CI 2.17–2.75). Data are representative of 2 experiments.

We hypothesized that a transition from WDLPS to DDLPS might involve reversal of the normal differentiation process from preadipocytes to adipocytes. To test this hypothesis, we compared differentially expressed genes in our LPS cell line samples with those in preadipocytes and adipocytes (gene expression data from Mikkelsen et al., ref. 25). Indeed, we noted significant overlap between these 2 data sets (P value $< 10^{-5}$). Among 3,516 downregulated genes in DDLPS cell lines and 1,129 downregulated genes in preadipocytes, 580 genes were common to both data sets (Figure 2A). Similarly, among 4,180 upregulated genes in DDLPS cell lines and 1,100 upregulated genes in preadipocytes, 454 genes were common to both data sets (Figure 2C). GSEA of these commonly

differentially expressed genes (580 commonly downregulated and 454 commonly upregulated genes in DDLPS cell lines and preadipocytes compared with WDLPS cell lines and adipocytes, respectively) again highlighted pathways involved in cellular differentiation, epigenetic enzyme targets, lipid metabolism, metastasis, and cell cycle (Figure 2, B and D, and Supplemental Tables 5 and 6). These data suggest that sarcoma cells may partially utilize genes similar to those used during normal differentiation processes.

KLF6 is a tumor suppressor that induces adipocytic differentiation and cellular senescence in DDLPS. Next, to understand the contribution of H3K9me3 changes to gene expression, we intersected the H3K9me3 ChIP-seq and expression microarray data sets. Of

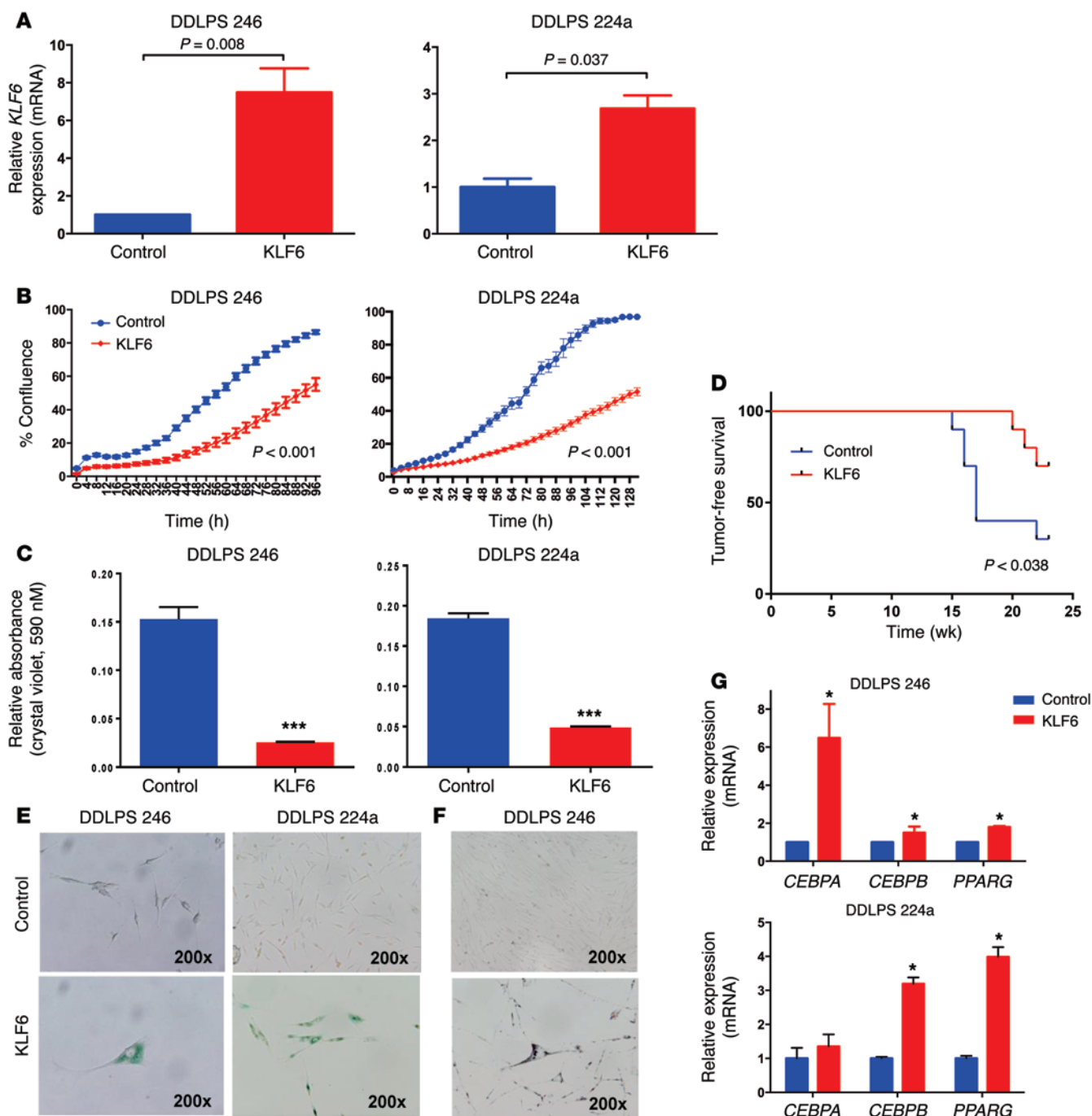


Figure 5. KLF6 overexpression inhibits DDLPS cell proliferation, induces expression of adipogenesis differentiation markers, and results in cellular senescence. (A) *KLF6* overexpression in DDLPS cell lines 246 and 224a, as assessed by qRT-PCR normalized to *GAPDH* (mean \pm SD; $n = 3$). Data were analyzed by Student's *t* test. (B) Cellular proliferation of DDLPS cell lines 246 and 224a overexpressing *KLF6* versus control (mean \pm SEM; $n = 10$). Data were analyzed by the Mann-Whitney *U* test. (C) Quantification of invaded cells from a Boyden chamber assay in DDLPS 246 and DDLPS 224a cells expressing control or *KLF6*. Plot shows relative absorbance of crystal violet staining in invaded cells (see images in Supplemental Figure 9, E and F) (mean \pm SEM; $n = 3$). Data were analyzed by Student's *t* test. (D) Tumor-free survival of mice s.c. injected with DDLPS 246 cells with stably expressing control (empty vector) or *KLF6*, as analyzed using the Kaplan-Meier method with the log-rank test ($n = 10$ per group). (E) β -Gal staining for cellular senescence in DDLPS cell lines 246 and 224a overexpressing *KLF6* versus control. (F) Oil red O staining for intracellular lipid accumulation in DDLPS cell line 246 overexpressing *KLF6* versus control. (G) Relative expression of adipogenesis-associated markers *CEBPA*, *CEBPB*, and *PPARG* in DDLPS cell lines 246 and 224a overexpressing *KLF6* versus control, as assessed by qRT-PCR normalized to *GAPDH* (mean \pm SD; $n = 3$). Data were analyzed by Student's *t* test and are representative of 2 experiments. * $P < 0.05$; *** $P < 0.001$.

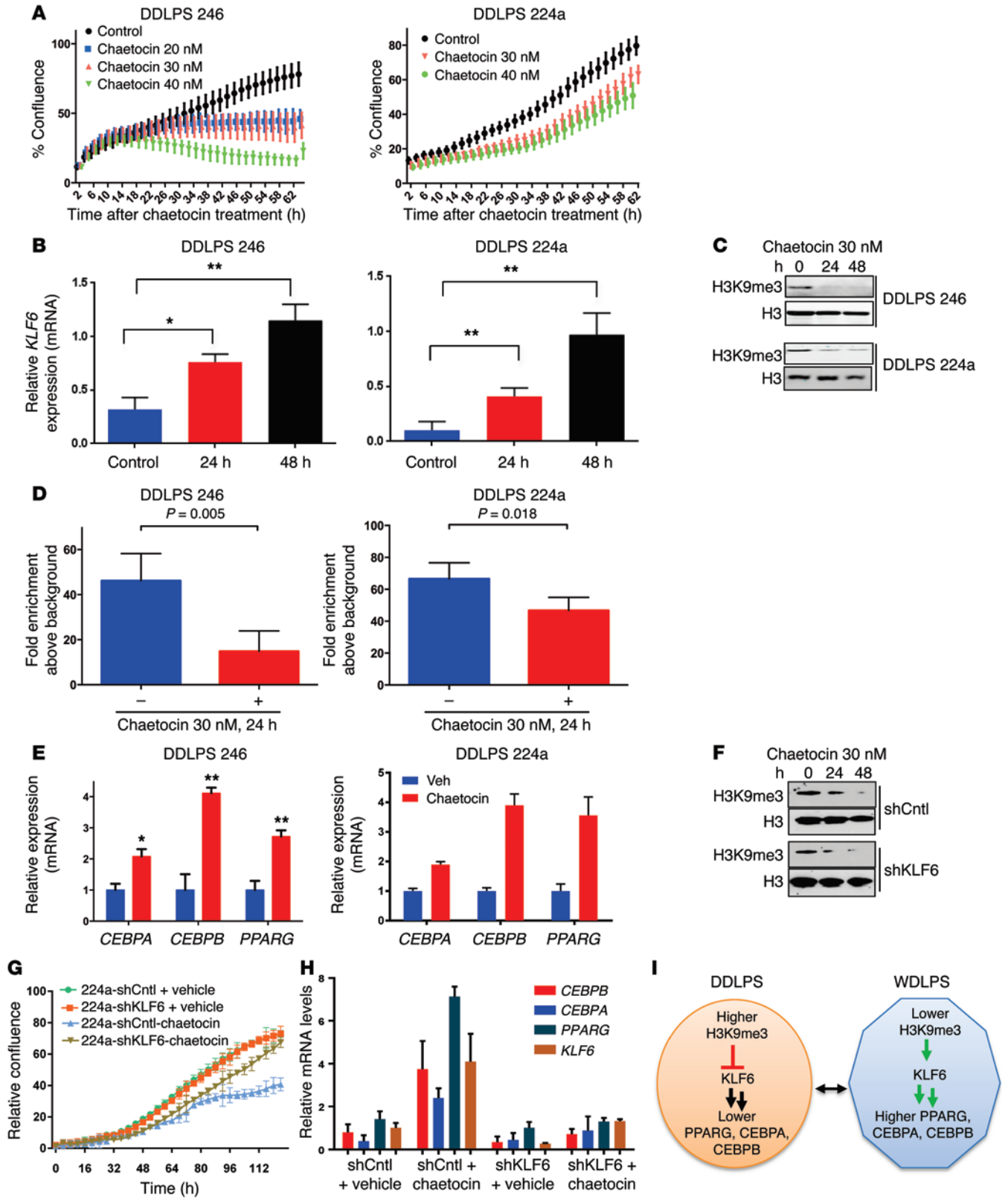


Figure 6. Chaetocin, an inhibitor of SUV39H1, inhibits DDLPS proliferation, inhibits H3K9 trimethylation globally and at the *KLF6* locus, and induces upregulation of *KLF6* and the proadipogenic factors *PPARG*, *CEBPA*, and *CEBPB*. (A) Proliferation of DDLPS cell lines 246 and 224a upon chaetocin treatment (mean \pm SEM; $n = 6$). Data were analyzed by 2-way ANOVA. (B) *KLF6* expression by qRT-PCR analysis in DDLPS cell lines 246 and 224a following chaetocin treatment (30 nM), normalized to *GAPDH* (mean \pm SD, $n = 3$). Data were analyzed by Student's *t* test. (C) Global levels of H3K9me3 by Western blot analysis in DDLPS cell lines 246 and 224a following chaetocin treatment (30 nM). (D) ChIP-qPCR analysis of H3K9me3 enrichment at the *KLF6* locus in DDLPS 246 and 224a cells treated with vehicle versus chaetocin (30 nM) for 24 hours (mean \pm SD, $n = 3$). Data were analyzed by Student's *t* test. (E) Relative expression of *PPARG*, *CEBPA*, and *CEBPB* by qRT-PCR in DDLPS cell lines 246 and 224a following chaetocin treatment (30 nM) for 24 hours, normalized to *GAPDH* (mean \pm SD, $n = 3$). Data were analyzed by Student's *t* test. (F) Global levels of H3K9me3 by Western blot analysis in DDLPS 224a stably expressing a control shRNA (shCntl) or *KLF6* shRNA (sh*KLF6*) following chaetocin treatment (30 nM). (G) Proliferation of DDLPS 224a stably expressing a control shRNA (shCntl) or *KLF6* shRNA (sh*KLF6*) upon chaetocin treatment (mean \pm SEM; $n = 6$). (H) Relative expression of *PPARG*, *CEBPA*, and *CEBPB* by qRT-PCR in DDLPS 224a stably expressing a control shRNA (shCntl) or *KLF6* shRNA (sh*KLF6*) following chaetocin treatment (30 nM) for 24 hours, normalized to *GAPDH* (mean \pm SD, $n = 3$). (I) Proposed model of *KLF6* as a differentially expressed and epigenetically (H3K9me3) regulated transcription factor with a tumor-suppressive role in LPS. In DDLPS relative to WDLPS, higher H3K9me3 levels at the *KLF6* locus suppresses *KLF6* expression, resulting in decreased expression of the proadipocytic regulators *PPAR γ* , *CEBP α* , and *CEBP β* . Data are representative of 2 experiments. * $P < 0.05$; ** $P < 0.001$.

243 regions with increased H3K9me3 enrichment in DDLPS cells relative to WDLPS cells, 121 regions were within 25 kb of 145 genes. Of these genes, 10 were differentially downregulated in DDLPS cells (Figure 3A). Similarly, of 17 regions with decreased H3K9me3 enrichment in DDLPS cells compared with WDLPS cells, 11 regions were within 25 kb of 16 genes. Of these genes, 5 were differentially upregulated in DDLPS cells (Figure 3B).

Among the 10 genes (*KLF6*, *TBC1D1*, *DUSP1*, *FRMD6*, *AMOTL2*, *HAL*, *PPP4R1*, *MTHFS*, *GTPBP4*, and *CAB39*) with H3K9me3 enrichment and expression downregulation in DDLPS cells compared with WDLPS cells, *KLF6* stood out as one with a known tumor-suppressor role in cancers (26) implicated in processes including adipogenesis, cell migration, metastasis, cell cycle regulation, and apoptosis. While the full-length form of *KLF6* (*KLF6-wt*) functions as a tumor suppressor, *KLF6* splice variant 1 (*KLF6-sv1*) is an oncogenic splice variant that functions in a dominant-negative fashion and has been shown to be overexpressed across multiple human malignancies, including glioblastoma, prostate, liver, pancreatic, lung, ovarian, and breast cancers (27–32). Given the evidence from the above-cited literature and our observation of enriched H3K9me3 at the regulatory region of *KLF6*, with associated underexpression in DDLPS cell lines compared with WDLPS cell lines (Figure 3, C and D, and Supplemental Figure 6, A and B), we selected *KLF6* for further studies to elucidate its role(s) in LPS.

To first reinforce the relevance of *KLF6* in human LPS, we assessed expression levels of *KLF6* in an independent set of samples that were surgically resected WDLPS ($n = 14$) and DDLPS ($n = 18$) tumors as well as normal fat ($n = 8$). Here, we measured expression levels of total *KLF6*, *KLF6-wt*, and *KLF6-sv1* by quantitative RT-PCR (qRT-PCR) using transcript-specific primers. As shown

in Figure 4A (and Supplemental Figure 7A), *KLF6* was significantly underexpressed in DDLPS tumors compared with expression levels detected in WDLPS tumors ($P < 0.001$) and normal fat ($P = 0.008$), while the dominant-negative isoform *KLF6-sv1* was not overexpressed in DDLPS tumors compared with WDLPS tumors (Supplemental Figure 7B). Correspondingly, Western blot analysis of the same WDLPS and DDLPS tumors and normal fat specimens showed that *KLF6* was significantly underexpressed in DDLPS tumors compared with WDLPS tumors ($P < 0.001$) and normal fat (Figure 4B and Supplemental Figure 8C). Relative median and mean *KLF6* protein levels (expressed as band intensity normalized to the sample T25 signal) were 2.39 and 33.50 in normal fat samples, 0.65 and 6.99 in DDLPS tumors, and 11.15 and 31.44 in WDLPS tumors.

To exclude genomic copy number alterations accounting for differential expression of *KLF6*, we determined the copy numbers of *KLF6* in genomic DNA extracted from WD and DD sarcoma cell lines and LPS tumors by qPCR. Among the cell lines, there was no significant difference in relative *KLF6* copy numbers between DDLPS and WDLPS cell lines (Figure 4C). While median *KLF6* copy numbers in normal fat samples relative to those in WDLPS tumors and DDLPS tumors showed no statistically significant difference (Figure 4D), a slight increase in relative copy numbers between WDLPS and DDLPS tumors was observed (2.04 vs. 2.46, $P = 0.012$), although we do not believe that this difference alone could account for the marked differences in *KLF6* protein expression levels, both between the 2 histologic tumor types and within a given tissue or tumor type (Supplemental Figure 8).

To ascertain whether gene mutation might contribute to differential *KLF6* expression, we performed whole-exome sequencing and mutational analysis of genomic DNA extracted from normal fat ($n = 2$) and WDLPS ($n = 14$) and DDLPS ($n = 19$) tumor specimens. No truncating mutations were identified that would account for differences in *KLF6* expression between DDLPS and WDLPS tumors (data not shown). Taken together, these data suggest that *KLF6* expression is suppressed in DDLPS samples (compared with WDLPS) by higher levels of H3K9me3 in *cis*-regulatory regions.

To assess the LPS-relevant activities of *KLF6*, we generated 3 stable DDLPS cell lines (DDLPS 224a, DDLPS 224b, and DDLPS 246) overexpressing *KLF6* (Figure 5A and Supplemental Figure 9A). DDLPS cells overexpressing *KLF6* exhibited decreased proliferation rates (Figure 5B and Supplemental Figure 9B) and decreased invasiveness in vitro (Figure 5C and Supplemental Figure 9, C–F). Consistent with these results from in vitro assays, DDLPS 246 cells overexpressing *KLF6* formed tumors with significantly longer latency in nude mice (Figure 5D). Further, *KLF6*-overexpressing cells also appeared to undergo morphological and phenotypic changes consistent with cellular senescence (Figure 5E and Supplemental Figure 9G) and suggestive of adipocytic differentiation, exhibiting increased size with accumulation of cytosolic lipid droplets detected by oil red O staining (Figure 5F). Molecularly, this phenotypic change is associated with increased expression of *PPARG*, the “master regulator” of adipogenesis, as well as of genes encoding the proadipogenic transcription factors *CEBP α* and *CEBP β* (Figure 5G and Supplemental Figure 9H).

Taken together, these data suggest that *KLF6* is a novel tumor suppressor in LPS that functions to inhibit cellular proliferation and invasion and drive senescence and differentiation through the regulation of master regulators of adipogenesis.

Pharmacologic inhibition of the H3K9me3 mark in DDLPS cell lines blocks proliferation and drives adipogenic differentiation. To test the functional role of H3K9me3 marks in DDLPS, we used a pharmacologic strategy to inhibit H3K9me3 in DDLPS and assayed the resulting impact on cellular phenotypes and *KLF6* expression. Chaetocin is a reported inhibitor of SUV39H1, the histone lysine methyltransferase responsible for H3K9 trimethylation, with an IC_{50} of 0.8 μ M (33). We treated DDLPS cell lines with vehicle control or increasing concentrations of chaetocin and assessed the impact on cell survival and proliferation. Across DDLPS cell lines (DDLPS 246, 224a, and 224b), we found that chaetocin inhibited cellular proliferation (Figure 6A and Supplemental Figure 10A), with an IC_{50} of approximately 30 to 40 nM (Supplemental Figure 11). Interestingly, the sensitivity of DDLPS cell lines to chaetocin and the global increase in H3K9me3 in DDLPS tumors compared with WDLPS tumors seen by IHC (Table 1) were not attributable to *SUV39H1* expression at the transcriptional level, as no differential expression in mRNA levels was observed in either LPS cell lines or tumors (Supplemental Figure 12, A and B). Moreover, normal fat and DDLPS and WDLPS tumors harbored similar levels of other known H3K9 methyltransferases and demethylases, except for *KDM4A*, which had intriguingly higher expression levels in DDLPS tumors (that also bore higher levels of H3K9me3) (Supplemental Figure 12, C-K).

Next, to test whether the growth inhibitory effect of chaetocin treatment on DDLPS cell lines was associated with changes in H3K9me3 and *KLF6* expression levels, we profiled global H3K9me3 levels and *KLF6* expression in DDLPS cells upon treatment with chaetocin at 30 nM. As shown in Figure 6, growth inhibition by chaetocin treatment was accompanied by decreased H3K9me3 levels and a specific increase in *KLF6* mRNA expression levels (Figure 6, B and C, and Supplemental Figure 10, B and C). To confirm that this change in global H3K9me3 levels upon chaetocin treatment (30 nM, 24 h) was indeed regulating *KLF6* expression, we performed an orthogonal ChIP-qPCR assay for H3K9me3 at the previously identified *KLF6*-associated regulatory region (Figure 3C and Supplemental Figure 6A). Indeed, we found that there was a significant decrease in H3K9me3 at this region in DDLPS cells treated with chaetocin (Figure 6D and Supplemental Figure 10D). Importantly, this decrease in H3K9me3 at the *KLF6*-associated regulatory region and the consequent increase in *KLF6* expression upon chaetocin treatment were associated with significant increases in mRNA expression levels of the known adipogenesis regulators *PPARG*, *CEBPA*, and *CEBPB* (Figure 6E and Supplemental Figure 10E).

Finally, to determine whether *KLF6* is a functional intermediary of chaetocin-mediated phenotypic and molecular changes, we knocked down *KLF6* in DDLPS 224a cells and tested the effect of chaetocin on the proliferation and expression levels of differentiation regulators. Indeed, cells harboring sh*KLF6* were refractory to the effect of chaetocin; in other words, no significant difference was observed between the control and chaetocin-treated cells upon *KLF6* knock down. Similarly, vehicle- and

chaetocin-treated cells harbored similar levels of *CEBPA* and *PPARG* (Figure 6, F-H). These data demonstrate that the effect of chaetocin on the proliferation and expression of differentiation regulators is in part dependent on *KLF6*, consistent with a causative role for *KLF6* and the observed differences in H3K9me3 levels between DDLPS and WDLPS cells.

Discussion

In this study, a systematic global analysis of 9 epigenetic modifications in WDLPS and DDLPS tumors from patients identified H3K9me3 as a chromatin mark that is differentially enriched between the 2 types of LPS. Integrated epigenomic and transcriptomic analyses revealed a repressive chromatin signature at the *KLF6* locus that resulted in downregulation of *KLF6* expression in DDLPS tumor cells (Figure 6I). Clinicopathological validation confirmed that *KLF6* is underexpressed in tumors from patients with DDLPS relative to normal fat and WDLPS tumors. Functional validation confirmed tumor-suppressive activity of *KLF6* in senescence and differentiation, in part through known regulators of adipogenesis such as *PPARG*. Pharmacologic inhibition of H3K9me3 marked in DDLPS cell line models resulted in a decrease in the repressive mark H3K9me3 at the *KLF6* locus and coordinated upregulation of *KLF6* expression. Taken together, we conclude that higher levels of H3K9me3 are associated with an aggressive dedifferentiated type of LPS and in part function by epigenetically silencing *KLF6*, a previously unknown tumor suppressor in LPS.

We believe that our results provide new insights into liposarcogenesis and suggest that the transition between WD and DD LPS subtypes might involve already existing networks utilized during normal adipocytic differentiation. Recent studies have established the role of *PPAR γ* as a master regulator of adipogenesis (34). Genome-wide binding profiles of *PPAR γ* have revealed a number of binding sites and shown that it binds to different sites in different cell types and hence plays important roles in lineage determination. Many *PPAR γ* -bound sites are located far from proximal promoters, and some of these sites overlap with super-enhancers — defined as large clusters of transcriptional enhancers that drive expression of cell identity-determining genes. *PPAR γ* -bound super-enhancers loop not only to the nearest promoter but also to distant promoters to activate transcriptional programs downstream in the *PPAR γ* -regulatory network (23, 35). Interestingly, one of the *KLF6*-associated regulatory regions showing differential H3K9me3 levels in WDLPS and DDLPS is located within a region previously characterized as an adipose-associated super-enhancer (23). Moreover, acquisition of a differentiated molecular phenotype upon chaetocin treatment in DDLPS cells is associated with loss of the H3K9me3 mark at this region. It may be speculated that H3K9me3 loss opens up the chromatin at certain super-enhancer regions, thereby helping with proadipogenic transcriptional reprogramming.

Although it is formally possible that relative changes in H3K9me3 levels between WDLPS and DDLPS cells are part of a differentiation program, our studies showing that chaetocin treatment diminishes the proliferative abilities of DDLPS cells and results in upregulation of differentiation regulators and that *KLF6* knockdown abrogates the effects of chaetocin treatment suggest that *KLF6* is a major downstream effector of differential

H3K9me3 levels. Our data in the context of the aforementioned studies strongly argue for a role of KLF6 in regulating and maintaining adipocytic differentiation in WDLPS (relative to DDLPS) and suggest that H3K9me3-mediated repression of KLF6 results in a failure to maintain normal adipocytic differentiation during DD liposarcomagenesis. It is interesting to note that KLF6 levels in WDLPS tumors were not only higher than those in DDLPS tumors but also than those in normal fat, an observation that should be further investigated. KLF6 is a transcription factor belonging to the family of Kruppel-like zinc finger transcription factors that has been implicated in a number of processes including adipogenesis, cell motility/invasion, cell cycle regulation, and apoptosis (26). KLF6 is upregulated during the differentiation process from preadipocytes to adipocytes (36) and acts as a transcriptional repressor of important genes such as the proto-oncogene Delta-like 1 (*DLK1*), which otherwise would lead to repression of PPAR γ (37). Additional suggested mechanisms for the tumor-suppressor function of *KLF6* include transactivation of p21 in a p53-independent manner (31), reduction of cyclin D1-CDK4 complexes via interaction with cyclin D1 (38), and inhibition of c-Jun proto-oncoprotein activities (39). Indeed, all of these pathways are known to be dysregulated in LPS (5).

Overall, this study highlights the value of applying epigenomic approaches as a discovery platform to identify novel targets in liposarcomagenesis and identifies H3K9me3 as an important marker associated with aggressive DDLPS. Our study warrants further evaluation of the use of H3K9me3 inhibitors as agents to reduce the aggressiveness of DDLPS. Importantly, we introduce *KLF6* as a previously undescribed tumor suppressor in LPS that is differentially expressed and epigenetically regulated, at least in part, between WDLPS and DDLPS. Future studies to elucidate mechanisms by which the *KLF6* locus is targeted for differential H3K9 trimethylation as well as the pathways by which KLF6 mediates its proadipocytic differentiation effects will be critically important and of great potential therapeutic importance in a cancer for which our understanding is limited and for which the only means of disease control is often repeated and highly morbid surgical resection and/or debulking of initial and recurrent tumors.

Methods

IHC. A TMA consisting of cores derived from WDLPS and DDLPS formalin-fixed, paraffin-embedded (FFPE) tissue specimens (from 151 patients) and normal fat was constructed as previously described (13, 40). IHC was performed using anti-H3K9me3 (1:1,000), anti-H3K27Ac (1:1,000), anti-H3K20me3 (1:1,000), and anti-H3K36me2 (1:1,000) from Abcam (catalog/lot numbers ab8898/GR25650, ab4729/GR28402-1, ab9053/GR5014-1, and ab9049/GR2471-1); anti-5mC (1:1,000) from Eurogentec (catalog BI-MECY-0100/100615); anti-5hmC (1:2,000) and anti-H3K4me3 (1:1,000) from Active Motif (catalogs 39769/1031001 and 39159/01609004); and anti-H3K27me3 (1:1,000) and anti-H3K79me3 (1:1,000) from EMD Millipore (catalogs 07-449/2148525 and CS204342/205140). TMA slides were heated at 65°C for 2 hours, deparaffinized in xylene, and rehydrated. Antigen retrieval was performed by steaming the slides in sodium citrate buffer (10 mM sodium citrate, 0.05% Tween-20, pH 6.0) at 95°C for 30 minutes and 90°C for 30 seconds. After cooling, the slides were incubated in 3% H₂O₂ for 20 minutes, washed in PBS,

and blocked overnight at 4°C in goat serum. After incubation with a primary antibody for 1 hour at 37°C, a secondary antibody was applied for 30 minutes at 37°C. The slides were then washed, incubated in VECTASTAIN Elite ABC reagent (Vector Laboratories), and developed using DAB reagent (Vector Laboratories). The slides were then dehydrated and the coverslips mounted.

Immunohistochemical stains of TMA slides were interpreted by soft tissue and bone pathologists (G.A. Al Sanna and A.J. Lazar), who scored the mean stain intensity (0 = negative, 1 = low, 2 = intermediate, 3 = high) and percentage of tumor cells stained (0%–100%). For each core, the mean stain intensity score and percentage of tumor stained score were multiplied to derive a multiplier score. To test whether epigenetic marker expression differed between LPS histologies, we used the Kruskal-Wallis test, a nonparametric multigroup comparisons test. Statistical analyses were performed using IBM SPSS Statistics 19.

ChIP. ChIP was performed as described earlier (41). Cells (5 million per antibody) were cross-linked using 1% paraformaldehyde for 10 minutes at 37°C. Reactions were quenched by 0.125 M glycine for 5 minutes. Cells were then washed with PBS and stored at –80°C. Cells were thawed on ice the next day and lysed with radioimmunoprecipitation assay (RIPA) buffer (10 mM Tris-HCl pH 8.0, 1 mM EDTA, pH 8.0, 140 mM NaCl, 1% Triton X-100, 0.2% SDS, 0.1% deoxycholic acid (DOC) for 10 minutes on ice. Sonication was performed using the Branson Sonifier 250 to achieve a DNA shear length of 200 to 500 bp. Extracts were then incubated overnight with their respective antibody-Dynabead (Life Technologies) mixture (previously incubated together for 1 hour at 4°C [Rabbit IgG and H3K9me3, both from Abcam]). Immune complexes were then washed 3 times with RIPA buffer, once with RIPA-500 (RIPA with 500 mM NaCl), and once with LiCl wash buffer (10 mM Tris-HCl, pH 8.0, 1 mM EDTA, pH 8.0, 250 mM LiCl, 0.5% NP-40, 0.5% DOC). Elution and de-cross-linking were performed in direct elution buffer (10 mM Tris-Cl, pH 8.0, 5 mM EDTA, 300 mM NaCl, 0.5% SDS) by incubating immune complexes at 65°C for 4 to 16 hours. Treatment with proteinase K (20 mg/ml) and RNaseA was performed and DNA cleaned up using AMPure beads (Beckman-Coulter).

Next-generation sequencing. Sequencing library preparation was performed using New England BioLabs reagents as described earlier (41). Sequencing was performed using the HiSeq 2000 system (Illumina). Bowtie (version 1.0.0; SourceForge) (42) was used to align H3K9Me3 ChIP-seq reads to the human genome assembly NCBI Build 37 (UCSC hg19) with the following parameters: -n 1 -m 1 --best-strata (uniquely mapped reads with 1 mismatch were retained). We first performed peak calling on individual samples, taking into consideration the respective input controls. Enriched regions were detected by Scripture package (43) with varying window sizes (750; 1,500; 5,000) and peaks were called ($P < 0.05$) (41). Collapsed repeat regions in the human genome (44) and “ultra-high signal suspect regions” identified by the ENCODE project (45) (<http://hgdownload.cse.ucsc.edu/goldenPath/hg19/encodeDCC/wgEncodeMapability/wgEncodeDacMapabilityConsensusExcludable.bed.gz>) were masked during the peak calling procedure. Called regions were merged with BEDTools (46). Intervals with a length of less than 350 bp and enriched regions in whole-cell extract samples were excluded from the final list. We then examined for regions specifically enriched in WD samples and not enriched in DD samples, and vice versa. Functional annotation of specific H3K9me3 regions was investigated by using the GREAT

algorithm (22) with the default association rule settings. A heatmap was drawn using the seqMINER tool (47) by dividing each H3K9me3 genomic location into 200 bins in 5-kb windows. Rank-based normalization was applied to binned results, and later, Kmeans clustering was performed for 2 clusters. Aggregate plots were generated using the NGSplot toolbox (<https://code.google.com/p/ngsplot/>) around identified H3K9me3 regions. Functional annotation of differentially expressed genes was ascertained using the HOMER software tool (24).

Generation of histograms of ChIP fragments across the *KLF6* locus in LPS cell lines was performed using the UCSC Genome Browser. Each track is normalized to 10 million reads, with the same track height and vertical viewing range within a given figure panel.

All data sets are publicly available in the NCBI's Gene Expression Omnibus (GEO) database (GEO GSE57754).

RNA Isolation and qRT-PCR. RNA was isolated using RNeasy and miRNeasy kits (QIAGEN). For qRT-PCR evaluation of gene expression, reverse transcription was performed to convert total RNA into single-strand cDNA using the SuperScript III system (Invitrogen, Life Technologies) prior to qPCR. SYBR label-based qPCR was performed on a Stratagene Real-Time PCR system and analyzed with the PCR system's software. *GAPDH* was used as an endogenous control. Primer sets were obtained from SABiosciences (QIAGEN).

***KLF6* sequencing.** Whole-exome sequencing of *KLF6* (Ensembl Gene ID ENSG00000067082, transcript ID ENST00000497571, and mutational analysis was performed at the MD Anderson Cancer Center Sequencing and MicroArray Core Facility).

Microarray and differential gene expression analysis. Microarray experiments were performed at the MD Anderson Center's ncRNA Sequencing Core Facility using the Affymetrix HG-U133A GeneChip platform. Preadipocyte and adipocyte gene expression data were retrieved from the GEO database (GEO GSE20752) (48). The robust multiarray average (RMA) method was used with default options (with background correction, quantile normalization, and log transformation) to normalize raw data from batches using R and Bioconductor's affy package (49). For genes represented by multiple probes on the array, the maximum expression value was retained for further analyses. A gene was called differentially expressed if the FDR-corrected *P* value was less than 0.05, which was calculated using the empirical Bayes method by eBayes function in Bioconductor's limma package. All data sets are publicly available in the NCBI's GEO database (GEO GSE57754).

Preparation of whole-tumor protein extracts. The frozen tissues used in the experiments were acquired under an IRB-approved protocol and were derived from surgically resected WDLPS and DDLPS samples and normal fat tissue. In all cases, WDLPS and DDLPS histology, as initially clinically diagnosed, was confirmed by soft tissue and bone pathologists (G.A. Al Sanna and A.J. Lazar). Furthermore, in all cases, 12q15/*MDM2* FISH was performed as previously described (6) and showed the expected 12q15/*MDM2* amplification. WDLPS and DDLPS tumor tissues and normal fat tissues were thawed on ice in NP-40 buffer (Boston BioProducts) containing cOmplete Protease Inhibitor Cocktail and phosSTOP tablets (Roche) and homogenized using the Next Advance Bullet Blender (speed 5; time, 5 min) and zirconium oxide beads (0.5 mm) according to the manufacturers' instructions. Cell lysates were collected and centrifuged for 15 minutes at 13,523 *g* to remove debris. The supernatant was collected and total protein concentration measured using the DC Protein Assay (Bio-Rad).

Histone acid extraction. Cells in tissue culture were washed twice with ice-cold PBS and resuspended in Triton Extraction Buffer (PBS with 0.5% Triton X-100, 0.02% NaN₃) containing cOmplete Protease Inhibitor Cocktail and phosSTOP tablets (Roche). Cells were lysed on ice for 10 minutes and then spun at 2,000 *g* for 10 minutes and the supernatant discarded. Cells were washed once in Triton extraction buffer, spun, and nuclei resuspended in 0.2N HCl and rotated overnight at 4°C for acid extraction of histones. Samples were then centrifuged at 2,000 *g* for 10 minutes, and the supernatant containing histone proteins was saved for protein content determination and Western blot analysis.

Western blot analysis. Western blot analysis was performed by standard methods using Invitrogen precast 4% to 12% gels. The primary antibodies used were anti-actin and anti-Flag (Sigma-Aldrich); anti-*KLF6* (catalog sc-7158; Santa Cruz Biotechnology Inc.); and anti-H3 and anti-H3K9me3 (both from Abcam). The secondary antibodies used were either obtained from LI-COR Biosciences and detected using the LI-COR Odyssey imager or were HRP-conjugated secondary antibodies obtained from Sigma-Aldrich and detected by chemiluminescence. Relative *KLF6* protein band intensities were quantified using ImageJ software (NIH).

Copy number variation analysis. Copy number variation (CNV) assays and data analysis were performed using the TaqMan Copy Number Assay for *KLF6* (Hs01231749_cn) and 2 reference assays (catalogs 4403326 and 4403316; Life Technologies) according to the manufacturer's instructions.

Cell culture and stable transduction of LPS cell lines. LPS cell lines were cultured in DMEM containing 10% FBS and maintained in standard tissue culture conditions (5% CO₂, 37°C). For *KLF6* overexpression, *KLF6* cDNA was cloned into the pCL-2x Flag destination vector using Gateway Technology (Invitrogen). pDONR-*KLF6* was obtained from Thermo Scientific (ORFeome collaboration human *KLF6* ORF with stop codon, accession number DQ890752). Retroviral particles were generated and packaged with the 293T cells using Lipofectamine 2000 (Invitrogen). LPS cell lines were then transduced and selected with puromycin (Life Technologies).

Drug treatment. Chaetocin (Sigma-Aldrich) was stored at -20°C as a 1-mM stock solution in DMSO and diluted to the indicated concentrations (Figure 6, A-H and Supplemental Figures 10 and 11) in cell culture media for experiments.

Proliferation, invasion, senescence, and oil red O assays. A cell proliferation assay was performed using the Incucyte instrument (Essen BioScience) and an integrated confluence algorithm as a surrogate for cell numbers. An invasion assay was performed using Boyden chambers (BD Biosciences) as previously described (6). The invaded cells were dissolved in 10% acetic acid for 30 minutes and absorbance measured at 590 nM. Cellular senescence and β-gal activity was assayed using a senescence detection kit (catalog K320-250; BioVision). For the oil red O assay, cells were washed with PBS, fixed in 4% paraformaldehyde for 10 minutes, and washed with PBS twice prior to staining with oil red O solution for 30 minutes. Cells were washed with distilled water prior to imaging.

Statistics. Statistical analyses were performed using GraphPad Prism (GraphPad Software) and IBM SPSS Statistics 19. Data represent the mean ± SEM or SD, as indicated. Differences between the means were analyzed using the 2-tailed unpaired Student's *t* test or ANOVA or the Mann-Whitney *U* or Kruskal-Wallis test. A *P* value of less than 0.05 was

considered significant. Significance values for differences in survival curves for mouse experiment were analyzed using the Mantel-Cox test.

Study approval. Patient samples were collected according to protocols (Lab06-0851 and Lab04-0890) approved by the IRB of The University of Texas MD Anderson Cancer Center.

Acknowledgments

The authors would like to thank Davis R. Ingram, Theresa Nguyen, and Kate Lynn Bill. This work was supported by grants from the NIH (T32CA009599, to E.Z. Keung, and 5K08CA160443-03, to K.E. Torres), the National Cancer Institute (1K99CA160578-01, to

K. Rai), and the Cancer Prevention and Research Institute of Texas (R1204, to L. Chin).

Address correspondence to: Kunal Rai, Department of Genomic Medicine, The University of Texas MD Anderson Cancer Center, 1515 Holcombe Blvd., Unit 1954, Houston, Texas 77030, USA. Phone: 713.792.6809; E-mail: krai@mdanderson.org. Or to: Lynda Chin, Department of Genomic Medicine, The University of Texas MD Anderson Cancer Center, 1515 Holcombe Blvd., Unit 1954, Houston, Texas 77030, USA. Phone: 713.792.6876; E-mail: lchin@mdanderson.org.

- Dei Tos AP. Liposarcoma: new entities and evolving concepts. *Ann Diagn Pathol.* 2000;4(4):252–266.
- Crago AM, Singer S. Clinical and molecular approaches to well differentiated and dedifferentiated liposarcoma. *Curr Opin Oncol.* 2011;23(4):373–378.
- Taylor BS, et al. Frequent alterations and epigenetic silencing of differentiation pathway genes in structurally rearranged liposarcomas. *Cancer Discov.* 2011;1(7):587–597.
- Horvai AE, DeVries S, Roy R, O'Donnell RJ, Waldman F. Similarity in genetic alterations between paired well-differentiated and dedifferentiated components of dedifferentiated liposarcoma. *Mod Pathol.* 2009;22(11):1477–1488.
- Coindre JM, Pedeutour F, Aurias A. Well-differentiated and dedifferentiated liposarcomas. *Virchows Arch.* 2010;456(2):167–179.
- Peng T, et al. An experimental model for the study of well-differentiated and dedifferentiated liposarcoma; deregulation of targetable tyrosine kinase receptors. *Lab Invest.* 2011;91(3):392–403.
- Ray-Coquard I, et al. Effect of the MDM2 antagonist RG7112 on the P53 pathway in patients with MDM2-amplified, well-differentiated or dedifferentiated liposarcoma: an exploratory proof-of-mechanism study. *Lancet Oncol.* 2012;13(11):1133–1140.
- Dickson MA, et al. Phase II trial of the CDK4 inhibitor PD0332991 in patients with advanced CDK4-amplified well-differentiated or dedifferentiated liposarcoma. *J Clin Oncol.* 2013;31(16):2024–2028.
- Luke JJ, et al. The cyclin-dependent kinase inhibitor flavopiridol potentiates doxorubicin efficacy in advanced sarcomas: preclinical investigations and results of a phase I dose-escalation clinical trial. *Clin Cancer Res.* 2012;18(9):2638–2647.
- Schwartz GK, et al. Phase I study of PD 0332991, a cyclin-dependent kinase inhibitor, administered in 3-week cycles (Schedule 2/1). *Br J Cancer.* 2011;104(12):1862–1868.
- Tseng WW, Somaiah N, Lazar AJ, Lev DC, Pollock RE. Novel systemic therapies in advanced liposarcoma: a review of recent clinical trial results. *Cancers (Basel).* 2013;5(2):529–549.
- Crago AM, et al. Copy number losses define subgroups of dedifferentiated liposarcoma with poor prognosis and genomic instability. *Clin Cancer Res.* 2012;18(5):1334–1340.
- Zhang P, et al. MiR-155 is a liposarcoma oncogene that targets casein kinase-1alpha and enhances β -catenin signaling. *Cancer Res.* 2012;72(7):1751–1762.
- Singer S, et al. Gene expression profiling of liposarcoma identifies distinct biological types/subtypes and potential therapeutic targets in well-differentiated and dedifferentiated liposarcoma. *Cancer Res.* 2007;67(14):6626–6636.
- Ugras S, et al. Small RNA sequencing and functional characterization reveals MicroRNA-143 tumor suppressor activity in liposarcoma. *Cancer Res.* 2011;71(17):5659–5669.
- Geutjes EJ, Bajpe PK, Bernards R. Targeting the epigenome for treatment of cancer. *Oncogene.* 2012;31(34):3827–3844.
- Rodriguez-Paredes M, Esteller M. Cancer epigenetics reaches mainstream oncology. *Nat Med.* 2011;17(3):330–339.
- Renner M, et al. Integrative DNA methylation and gene expression analysis in high-grade soft tissue sarcomas. *Genome Biol.* 2013;14(12):R137.
- Cedar H, Bergman Y. Linking DNA methylation and histone modification: patterns and paradigms. *Nat Rev Genet.* 2009;10(5):295–304.
- Baylin SB, Jones PA. A decade of exploring the cancer epigenome — biological and translational implications. *Nat Rev Cancer.* 2011;11(10):726–734.
- Cheng X, Blumenthal RM. Coordinated chromatin control: structural and functional linkage of DNA and histone methylation. *Biochemistry.* 2010;49(14):2999–3008.
- McLean CY, et al. GREAT improves functional interpretation of cis-regulatory regions. *Nat Biotechnol.* 2010;28(5):495–501.
- Hnisz D, et al. Super-enhancers in the control of cell identity and disease. *Cell.* 2013;155(4):934–947.
- Heinz S, et al. Simple combinations of lineage-determining transcription factors prime cis-regulatory elements required for macrophage and B cell identities. *Mol Cell.* 2010;38(4):576–589.
- Mikkelsen TS, et al. Comparative epigenomic analysis of murine and human adipogenesis. *Cell.* 2010;143(1):156–169.
- DiFeo A, Martignetti JA, Narla G. The role of KLF6 and its splice variants in cancer therapy. *Drug Resist Updat.* 2009;12(1):1–7.
- Difeo A, et al. KLF6-SV1 is a novel antiapoptotic protein that targets the BH3-only protein NOXA for degradation and whose inhibition extends survival in an ovarian cancer model. *Cancer Res.* 2009;69(11):4733–4741.
- Hartel M, et al. Increased alternative splicing of the KLF6 tumour suppressor gene correlates with prognosis and tumour grade in patients with pancreatic cancer. *Eur J Cancer.* 2008;44(13):1895–1903.
- Hatami R, et al. KLF6-SV1 drives breast cancer metastasis and is associated with poor survival. *Sci Transl Med.* 2013;5(169):169ra12.
- Narla G, et al. KLF6-SV1 overexpression accelerates human and mouse prostate cancer progression and metastasis. *J Clin Invest.* 2008;118(8):2711–2721.
- Narla G, et al. KLF6, a candidate tumor suppressor gene mutated in prostate cancer. *Science.* 2001;294(5551):2563–2566.
- Vetter D, et al. Enhanced hepatocarcinogenesis in mouse models and human hepatocellular carcinoma by coordinate KLF6 depletion and increased messenger RNA splicing. *Hepatology.* 2012;56(4):1361–1370.
- Greiner D, Bonaldi T, Eskeland R, Roemer E, Imhof A. Identification of a specific inhibitor of the histone methyltransferase SU(VAR)3-9. *Nat Chem Biol.* 2005;1(3):143–145.
- Leftorova MI, Haakonsson AK, Lazar MA, Mandrup S. PPAR γ and the global map of adipogenesis and beyond. *Trends Endocrinol Metab.* 2014;25(6):293–302.
- Siersbaek R, et al. Transcription factor cooperativity in early adipogenic hotspots and super-enhancers. *Cell Rep.* 2014;7(5):1443–1455.
- Inuzuka H, Nanbu-Wakao R, Masuho Y, Muramatsu M, Tojo H, Wakao H. Differential regulation of immediate early gene expression in preadipocyte cells through multiple signaling pathways. *Biochem Biophys Res Commun.* 1999;265(3):664–668.
- Zhou Y, Peng J, Jiang S. Role of histone acetyltransferases histone deacetylases in adipocyte differentiation adipogenesis. *Eur J Cell Biol.* 2014;93(4):170–177.
- Benzeno S, et al. Cyclin-dependent kinase inhibition by the KLF6 tumor suppressor protein through interaction with cyclin D1. *Cancer Res.* 2004;64(11):3885–3891.
- Slavin DA, Koritschoner NP, Prieto CC, Lopez-Diaz FJ, Chatton B, Bocco JL. A new role for the Kruppel-like transcription factor KLF6 as an inhibitor of c-Jun proto-oncoprotein function. *Oncogene.* 2004;23(50):8196–8205.
- Hwang JA, et al. Gankyrin is a predictive and oncogenic factor in well-differentiated and dedifferentiated liposarcoma. *Oncotarget.* 2014;5(19):9065–9078.
- Garber M, et al. A high-throughput chromatin immunoprecipitation approach reveals principles of dynamic gene regulation in mammals. *Mol*

- Cell*. 2012;47(5):810–822.
42. Langmead B, Trapnell C, Pop M, Salzberg SL. Ultrafast and memory-efficient alignment of short DNA sequences to the human genome. *Genome Biol*. 2009;10(3):R25.
43. Guttman M, et al. Ab initio reconstruction of cell type-specific transcriptomes in mouse reveals the conserved multi-exonic structure of lincRNAs. *Nat Biotechnol*. 2010;28(5):503–510.
44. Pickrell JK, Gaffney DJ, Gilad Y, Pritchard JK. False positive peaks in ChIP-seq and other sequencing-based functional assays caused by unannotated high copy number regions. *Bioinformatics*. 2011;27(15):2144–2146.
45. Consortium EP, et al. An integrated encyclopedia of DNA elements in the human genome. *Nature*. 2012;489(7414):57–74.
46. Quinlan AR, Hall IM. BEDTools: a flexible suite of utilities for comparing genomic features. *Bioinformatics*. 2010;26(6):841–842.
47. Ye T, et al. seqMINER: an integrated ChIP-seq data interpretation platform. *Nucleic Acids Res*. 2011;39(6):e35.
48. Barrett T, et al. NCBI GEO: archive for functional genomics data sets — update. *Nucleic Acids Res*. 2013;41(Database issue):D991–D995.
49. Irizarry RA, et al. Exploration, normalization, and summaries of high density oligonucleotide array probe level data. *Biostatistics*. 2003;4(2):249–264.